Central European Journal of Energetic Materials
ISSN 1733-7178; e-ISSN 2353-1843

Cent. Eur. J. Energ. Mater., 2016, *13*(3), 677-693; DOI: 10.22211/cejem/65015

Molecular Dynamics Simulation Studies of the CL-20/DNB Co-crystal

Ting SUN,[1] Ji Jun XIAO,[1*] Guang Fu JI,[2]
Feng ZHAO,[2] He Ming XIAO [1]

[1] *Molecules and Materials Computation Institute, School of Chemical Engineering, Nanjing University of Science and Technology, Nanjing 210094, P.R. China*
[2] *National Key Laboratory of Shock Wave and Detonation Physics, Institute of Fluid Physics, China Academy of Engineering Physics, Mianyang 621900, P.R. China*
[*] *E-mail: xiao_jijun@njust.edu.cn*

Abstract: Molecular dynamics (MD) simulation was conducted for a DNB (1,3-dinitrobenzene) crystal, a ε-CL-20 (2,4,6,8,10,12-hexanitro-2,4,6,8,10,12-hexaazaisowurtzitane) crystal, a CL-20/DNB co-crystal and a CL-20/DNB composite. From the calculated maximum bond length (L_{max}) of the N–NO_2 trigger bond, the cohesive energy density (*CED*) and the binding energy (E_{bind}), it was found that the CL-20/DNB co-crystal is more insensitive than its composite. Its thermal stability is also better than that of its composite. The pair correlation function (PCF) analysis method was applied to investigate the interfaces between different molecular layers in the CL-20/DNB co-crystal, and in the composite. Additionally, the calculated mechanical data showed that the moduli of the CL-20/DNB co-crystal and its composite are smaller and their elastic elongation and ductility are better than those of the ε-CL-20 and DNB crystals.

Keywords: CL-20/DNB co-crystal, composite, interactions, mechanical properties, molecular dynamics (MD) simulation

1 Introduction

In the field of energetic materials, high performance and insensitive explosives have always attracted much attention by researchers [1]. For the current single compound explosives, high performance and safety are somewhat

mutually exclusive, which seriously limits their development and applications [2]. Fortunately, the recent formation of energetic co-crystals [3-14] offers opportunities to modify the properties of energetic materials, such as oxygen balance, sensitivity, detonation velocity, and safety. A co-crystal [16, 17] is a multiple component crystal that is constructed from two or more neutral molecular components, which co-exist at an intrinsic stoichiometric ratio by non-covalent interactions (such as hydrogen bonding, van der Waals, and π–π stacking interactions, *etc*.).

2,4,6,8,10,12-Hexanitro-2,4,6,8,10,12-hexaazaisowurtzitane (CL-20, Figure 1a) is the most famous high energy density compound (HEDC) for practical applications at present, having high density, a good oxygen balance and high detonation velocity. The ε polymorph [18-20] of CL-20 crystals is the densest and most thermodynamically stable form of the reported crystalline forms (*α*, *β*, *γ* and ε). However, the ε-CL-20 crystal has also failed to meet the high demands of safety for modern ordnance due to its high sensitivity. Recently, researchers have attempted to reduce the sensitivity of ε-CL-20 crystals *via* the strategy of co-crystallization [5, 10-15], which reduces the sensitivity of ε-CL-20 crystals without a significant decrease in its energy performance. DNB (1, 3-dinitrobenzene, Figure 1b) is even more insensitive than TNT (2,4,6-trinitrotoluene), and is a well-known insensitive explosive [14, 21]. In this paper, we have studied a CL-20/DNB co-crystal, where the molar ratio is 1:1. This CL-20/DNB co-crystal features much better insensitivity and makes it a promising ingredient in CL-20 propellant formulations [14].

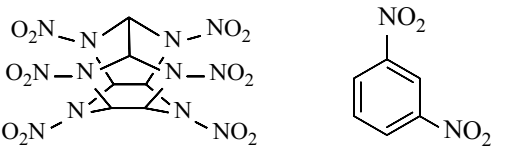

Figure 1. Molecular structures of: (a) CL-20, and (b) DNB.

For comparison, a CL-20/DNB composite with the same molar ratio as its co-crystal, ε-CL-20 and DNB crystals were also considered. It is well known that with increasing temperature, energetic materials become more sensitive and less stable. In view of this, molecular dynamics (MD) simulations were conducted at different temperatures. Structural data, cohesive energy densities (*CED*), binding energies (E_{bind}) and pair correlation functions (PCF) as well as the elastic properties were calculated from MD equilibrium trajectories. These

data were analyzed in order to compare and explore the sensitivity, thermal stability and mechanical properties of the materials.

This paper is arranged as follows. We first introduce the construction of the models and the computation conditions for the simulations. Then, the lattice parameters and the cell densities of the CL-20/DNB co-crystal at different temperatures are discussed and compared with experimental data to further verify that the COMPASS force field [22] is suitable for the MD simulation of the CL-20/DNB co-crystal. Subsequently, the $N{-}NO_2$ trigger bond lengths of the ε-CL-20 crystal, the CL-20/DNB composite and co-crystal at different temperatures are presented and discussed in order to disclose their relationship with sensitivity. *CED* and E_{bind} values between CL-20 and DNB molecules of the composite and the co-crystal are also provided and discussed in terms of their relationship with sensitivity and thermal stability. In addition, an analysis of the interaction of CL-20 and DNB molecules in the composite and the co-crystal is made by using PCF. Finally, mechanical properties such as tensile modulus (E), Poisson's ratio (ν), bulk modulus (K), shear modulus (G), the quotient K/G and the Cauchy pressure (C_{12}-C_{44}) are presented and discussed for the DNB crystal, the CL-20/DNB composite and co-crystal, and the ε-CL-20 crystal.

2 Modelling and Simulation Details

All simulations were conducted under the COMPASS (condensed-phase optimized molecular potentials for atomistic simulation studies) force field, which is suitable for MD simulations of nitramine- and nitro-compound explosives [23]. Based on the crystal parameters derived from X-ray diffraction [24, 25, 14], three primary simulation cells containing individually 72, 160 and 96 molecules, equivalent to 2592, 2560 and 2496 atoms, were used for the ε-CL-20, DNB crystals and the CL-20/DNB co-crystal, corresponding to 18 (2×3×3), 40 (2×2×10) and 6 (3×2×1) unit cells, respectively. In the co-crystal, the numbers of CL-20 and DNB molecules were both 48.

The simulation model for the CL-20/DNB composite was constructed as follows. The molar ratio of ε-CL-20 and DNB molecules was 1:1. Primary cells each containing 48 molecules were first built, having 12 (2×2×3) and 12 (2×1×6) unit cells for the ε-CL-20 and DNB crystals, respectively. The molecules in the ε-CL-20 and DNB primary cells were considered as two molecular clusters, and placed in a cubic box of length 100 Å. The cubic box was then compressed gradually and step by step; after each step the MD run at 295 K in a constant particle numbers, constant volume and constant temperature (NVT) ensemble

was performed until the system arrived at thermal equilibrium. The modelling of the composite was not completed until the density of the composite was close to its calculated value. The composite model contained 96 molecules, having a total of 2496 atoms.

The models of the ε-CL-20 and DNB crystals, the CL-20/DNB co-crystal and the composite were allowed to evolve dynamically in isothermal-isobaric (NPT) ensembles under Andersen temperature control using the stochastic collision method [26] and Parrinello-Rahman pressure control, fully relaxing all cell parameters [27] at atmospheric pressure. The temperature started from 195 K, increasing in increments of 50 K, to 395 K for the ε-CL-20 crystal and the CL-20/DNB co-crystal, and to 345 K for the DNB crystal and the CL-20/DNB composite due to the melting point (364 K) [21] of the DNB crystal. In the condensed phase simulation cases, van der Waals interactions were truncated at 9.5 Å with long range tail corrections [28], and electrostatic interactions were treated *via* the standard Ewald summation [29]. The motion equations were integrated with an increment of 1 fs. After an equilibration run, a production run of 1 ns was performed, during which data were collected with 10 fs sampling intervals for subsequent analysis. The computation for all of the materials was carried out using software program-MS (Material Studio) from Accelrys Inc. (San Diego, CA).

As an illustration, one equilibrium structure of the CL-20/DNB co-crystal and its composite at 295 K are shown in Figure 2.

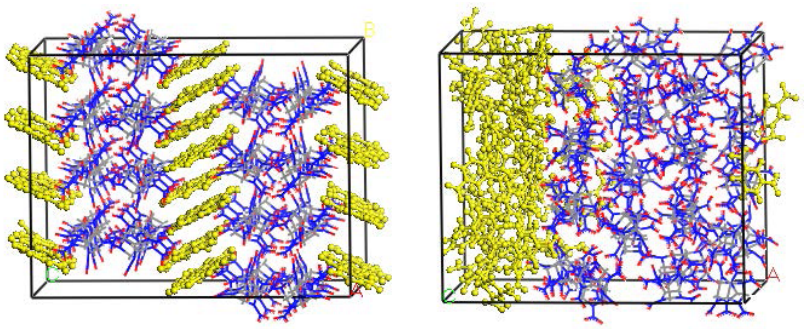

a b

Figure 2. Equilibrium structures of: (a) CL-20/DNB co-crystal, and (b) its composite.

3 Results and Discussion

3.1 Equilibrium lattice parameters and cell densities

The calculated lattice parameters and cell densities by MD simulations at different temperatures and one atmosphere pressure are summarized in Table 1 for the CL-20/DNB co-crystal, with comparison to experimental data. The experiment was performed at 293 K and one atmosphere pressure. A comparison of the simulation data at 295 K and the experimental data shows that the simulation lattice lengths (a, b, c) and cell density are slightly different and deviate by 0.5%, −4.8%, 4.3% and 0.5%, respectively. On the other hand, the interaxial angles (α, β, γ) hardly change with the temperature and are almost equal to the experimental values. Moreover, all of the lattice lengths increase gradually with increasing temperature, while the density changes trend is the opposite direction. This further confirms that the COMPASS force field [21] is suitable for MD simulation of the CL-20/DNB co-crystal.

Table 1. Equilibrium lattice parameters and cell densities of the CL-20/DNB co-crystal at different temperatures

Temperature [K]	a [Å]	b [Å]	c [Å]	α [°]	β [°]	γ [°]	ρ [g·cm^{-3}]
195	9.43	12.70	34.90	90.00	90.00	89.99	1.93
	(0.05)	(0.04)	(0.16)	(0.27)	(0.21)	(0.30)	(0.01)
245	9.47	12.75	34.98	90.01	90.00	90.00	1.91
	(0.05)	(0.05)	(0.16)	(0.32)	(0.24)	(0.35)	(0.01)
295	9.52	12.81	35.06	90.00	90.00	90.01	1.89
	(0.06)	(0.06)	(0.18)	(0.38)	(0.27)	(0.39)	(0.01)
345	9.57	12.92	35.14	89.72	90.00	89.97	1.85
	(0.08)	(0.07)	(0.22)	(0.51)	(0.30)	(0.44)	(0.01)
395	9.55	13.05	35.40	89.77	90.08	90.08	1.83
	(0.10)	(0.09)	(0.26)	(0.67)	(0.35)	(0.48)	(0.01)
Exp. [14]	9.47	13.46	33.62	90.00	90.00	90.00	1.88

Deviations are listed in parenthesis.

3.2 Trigger bond length and sensitivity

The sensitivity of energetic materials is the degree to which they can be initiated to explode by external stimuli. The trigger bond of energetic molecules breaks preferentially due to external stimuli, causing decomposition. Therefore, there is a significant correlation between sensitivity and trigger bond strength. Politzer *et al*. [30] have used the reciprocal of the lengths of the trigger bonds to measure

the bond strength and described the impact sensitivity of nitramine and nitro compounds. Since CL-20 is more sensitive than DNB, and both experimental and theoretical studies have verified that the trigger bond of CL-20 is N–NO_2 [31-34], in this study we are concerned with the trigger bond length of CL-20. The statistical distribution of bond length can be obtained via MD simulation based on the production trajectory, as shown in Figure 3. In the ε-CL-20 crystal, the average bond length (L_{ave}) of N–NO_2 is 1.397 Å, which is close to the experimental data of 1.369 Å [24] and the quantum optimized data of 1.371 Å [35]. On the other hand, considering that molecules having the maximum bond length are "activated" molecules, we have predicted the relative sensitivity of the energetic systems based on the maximum bond length (L_{max}) of the trigger bonds [36, 37].

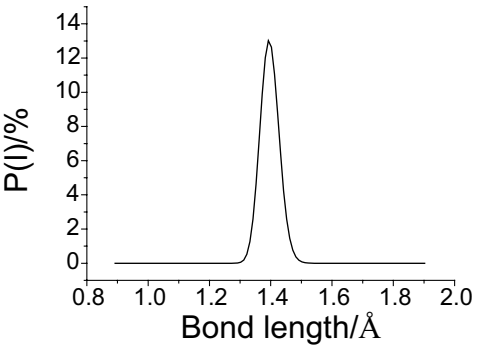

Figure 3. N–NO_2 bond length distribution of ε-CL-20 at 295 K.

Table 2. Trigger bond (N−NO_2) lengths of CL-20 in ε-CL-20 crystal, CL-20/DNB composite and the co-crystal at different temperatures

Model	Bond length [Å]	195 K	245 K	295 K	345 K	395 K
ε-CL-20	L_{ave}	1.395	1.396	1.397	1.398	1.399
		(0.025)	(0.028)	(0.031)	(0.033)	(0.036)
	L_{max}	1.544	1.568	1.592	1.617	1.638
Composite	L_{ave}	1.394	1.395	1.396	1.396	--
		(0.025)	(0.028)	(0.031)	(0.033)	--
	L_{max}	1.538	1.566	1.590	1.607	--
Co-crystal	L_{ave}	1.394	1.394	1.395	1.396	1.397
		(0.025)	(0.028)	(0.031)	(0.033)	(0.036)
	L_{max}	1.534	1.553	1.564	1.590	1.617

Deviations are listed in parenthesis.

Table 2 gives the trigger bond length (N–NO_2) of CL-20 molecules in the ε-CL-20 crystal, the CL-20/DNB composite and the co-crystal calculated from the production trajectory. As the temperature increases, L_{ave} of all three models increases slightly, while L_{max} increases gradually and significantly. Therefore, the change trend of L_{max} reflects well the fact that the sensitivity increases with higher temperatures. Furthermore, at the same temperature, L_{max} is compared as CL-20/DNB (co-crystal) < CL-20/DNB (composite) < ε-CL-20 (crystal). Therefore, we can rank the impact sensitivities of these systems in ascending order as CL-20/DNB (co-crystal) < CL-20/DNB (composite) < ε-CL-20 (crystal).

It was anticipated that adding DNB to ε-CL-20 would reduce the sensitivity relatively to ε-CL-20 itself by diluting the more sensitive component, whereas L_{max} reduction in the co-crystal is more significant than in the composite, suggesting that the co-crystal is less sensitive than the composite.

3.3 Molecular interactions in the CL-20/DNB co-crystal and the composite

3.3.1 Cohesive energy density of CL-20/DNB co-crystal and composite

The cohesive energy density (*CED*) is the amount of energy needed to completely separate molecules from each other per mole for unit volume until there are no interactions, *i.e.*, the energy required to transfer from the condensed phase to the gas phase. In atomistic simulations, the cohesive energy is defined as the energy needed for one mole of a material to reduce all intermolecular forces to zero, and the *CED* corresponds to the cohesive energy per unit volume. Thus, the *CED* is essentially a measurement of the intermolecular interactions among molecules in materials.

The calculated *CED* of the CL-20/DNB co-crystal and composite are listed in Table 3. The *CED* is the sum of the van der Waals (*vdW*) and electrostatic energy, *i.e.*, the nonbonded energies between molecules. Obviously, *CED*, *vdW*, and electrostatic energy all decrease monotonously with increasing temperature. This agrees with the experimental fact that sensitivity becomes higher with increasing temperature, as lower energy is required for material to transfer from the condensed phase to the gas phase, tending to cause easier decomposition and explosion [37]. Likewise, impact transfers mechanical energy to thermal energy and then the heat may in general cause decomposition and explosion. Therefore, the *CED* can also be used as a theoretical criterion for heat and impact sensitivity. At the same temperature, the *CED* of the co-crystal is obviously higher than that of the composite, indicating that the co-crystal is more stable, which is consistent with the result obtained from L_{max}.

Table 3. Cohesive energy density *CED* [a] and its component energies of CL-20/DNB composite and co-crystal at different temperatures (kJ/cm^3)

Model	Energy	Temperature, K									
		195		245		295		345		395	
Composite	*CED*	0.77	(0.01)	0.74	(0.01)	0.71	(0.01)	0.69	(0.01)	--	
	vdW	0.34	(0.00)	0.33	(0.00)	0.32	(0.00)	0.32	(0.00)	--	
	Electrostatic	0.42	(0.01)	0.41	(0.01)	0.39	(0.01)	0.37	(0.01)	--	
Co-crystal	*CED*	0.89	(0.01)	0.86	(0.01)	0.83	(0.01)	0.80	(0.01)	0.77	(0.01)
	vdW	0.43	(0.00)	0.41	(0.00)	0.40	(0.00)	0.38	(0.00)	0.37	(0.00)
	Electrostatic	0.46	(0.01)	0.45	(0.01)	0.43	(0.01)	0.42	(0.01)	0.40	(0.01)

[a] $CED = E_{vdW} + E_{Electrostatic}$. Deviations are listed in parenthesis.

3.3.2 Binding energy between CL-20 and DNB molecules in the CL-20/DNB co-crystal and composite

The binding energy (E_{bind}) is defined as the negative value of the intermolecular interaction energy (E_{inter}), that is, $E_{bind} = -E_{inter}$, which can reflect well the miscibility of the two components blended with each other. A higher binding energy means a stronger interaction between components and thus a more stable system. The intermolecular interaction energy can be evaluated from the total energy of the whole system and the individual component energies in the system. As such, E_{bind} between CL-20 and DNB molecules can be expressed as follows.

$$E_{bind} = - E_{inter} = - (E_{total} - E_{CL\text{-}20} - E_{DNB})$$

where E_{total} is the total energy of the whole system, and $E_{CL\text{-}20}$ and E_{DNB} are the energies of the CL-20 and DNB molecules, respectively. In this paper, it has an important influence on the miscibility for the CL-20/DNB composite, the formation of the co-crystal and the thermal stability of the energetic systems.

E_{bind} and its components of the composite and the co-crystal at different temperatures are tabulated in Table 4. E_{bind} is equal to the nonbonded energy because the internal energy difference is zero. The nonbonded energy is derived from the *vdW* and electrostatic energies. Considering that the electrostatic energy is much larger than the *vdW* energy for both the composite and the co-crystal, we can know that the interaction between the CL-20 and DNB molecules is mainly from the contribution of the electrostatic interactions. It is noticed that E_{bind} and its components decrease monotonously with increasing temperature, which means

that the thermodynamic stability of the system decreases. Furthermore, E_{bind} of the co-crystal is much larger than that for the composite at the same temperature, which means that the co-crystal is more stable. This can be explained from Figures 2a and 2b, where it can be seen that the DNB layer is placed alternately between CL-20 bilayers in the co-crystal, and interactions exist between the two layers, while in the CL-20/DNB composite, the interface area of different components is much smaller. Thus, it is not difficult to understand that the interaction between the DNB and CL-20 molecules in the co-crystal is stronger. Also, compared with Table 3, E_{bind} differences between the co-crystal and the composite are much larger than that of the *CED* at the same temperature, implying that the dependence of E_{bind} on spatial molecular ordering is greater than that of the *CED*.

Table 4. Binding energies and the component energies of CL-20/DNB (composite and co-crystal) at different temperatures

Model	Energy [kJ/mol]	195 K		245 K		295 K		345 K		395 K	
Composite	E_{bind}	67.3	(-1.0)	65.8	(-0.5)	63.9	(-1.1)	59.9	(-1.8)	--	
	Internal	0.0	(0.0)	0.0	(0.0)	0.0	(0.0)	0.0	(0.0)	--	
	Non-bonded	67.3	(-1.0)	65.8	(-0.5)	63.9	(-1.1)	59.9	(-1.8)	--	
	vdW	26.4	(-0.4)	26.0	(-0.5)	24.7	(-0.5)	24.9	(-0.7)	--	
	Repulsive	-64.9	(-2.4)	-62.7	(-1.8)	-60.3	(-3.1)	-56.0	(-3.4)	--	
	Dispersive	91.2	(-2.2)	88.7	(-1.7)	85.0	(-2.7)	80.9	(-2.9)	--	
	Electro-static	40.9	(-1.2)	39.8	(-0.4)	39.2	(-1.5)	35.0	(-1.7)	--	
Co-crystal	E_{bind}	128.5	(-1.1)	126.5	(-1.1)	124.5	(-1.2)	116.9	(-1.6)	112.2	(-1.5)
	Internal	0.0	(0.0)	0.0	(0.0)	0.0	(0.0)	0.0	(0.0)	0.0	(0.0)
	Non-bonded	128.5	(-1.1)	126.5	(-1.1)	124.5	(-1.2)	116.9	(-1.6)	112.2	(-1.5)
	vdW	43.0	(-0.5)	42.0	(-0.9)	41.5	(-1.2)	40.0	(-1.0)	39.2	(-1.2)
	Repulsive	-135.5	(-2.3)	-132.1	(-2.2)	-130.3	(-4.8)	-120.7	(-4.6)	-112.6	(-3.1)
	Dispersive	178.5	(-2.5)	174.1	(-1.8)	171.8	(-3.9)	160.8	(-4.2)	151.8	(-2.3)
	Electro-static	85.5	(-1.1)	84.5	(-0.8)	83.0	(-1.3)	76.9	(-1.9)	73.1	(-1.3)

$E_{bind} = E_{internal} + E_{Nonbond}$; $E_{Nonbond} = E_{vdW} + E_{Electrostatic} = E_{Repulsive} + E_{Dispersive} + E_{Electrostatic}$.
Deviations are listed in parenthesis.

3.3.3 Pair correlation function (PCF) for the CL-20/DNB co-crystal and composite

To explore the interactions between molecules in the CL-20/DNB co-crystal and composite, molecular surface electrostatic potentials was the method adopted, which is based on quantum mechanics calculations [39, 40], while the PCF

function was used in this work where classical MD simulations were conducted.

The PCF gives an insight into the structure of the material through a measure of the local spatial ordering, and uses a measure of conditional number probability density $g(r)$ for finding an atom at certain distances from a reference atom. In the present work, three atom pairs (H···O, H···N and C···O) were considered. H, O, and N (negatively charged) atoms in CL-20 molecules were denoted by H(1), O(1), and N(1), and H, O, C atoms in DNB molecules as H(2), O(2) and C(2), respectively. In order to explore the interactions between the CL-20 and DNB molecules, PCFs of H···O, H···N and C···O atomic pairs in the CL-20/DNB co-crystal and composite at 295 K are plotted in Figure 4.

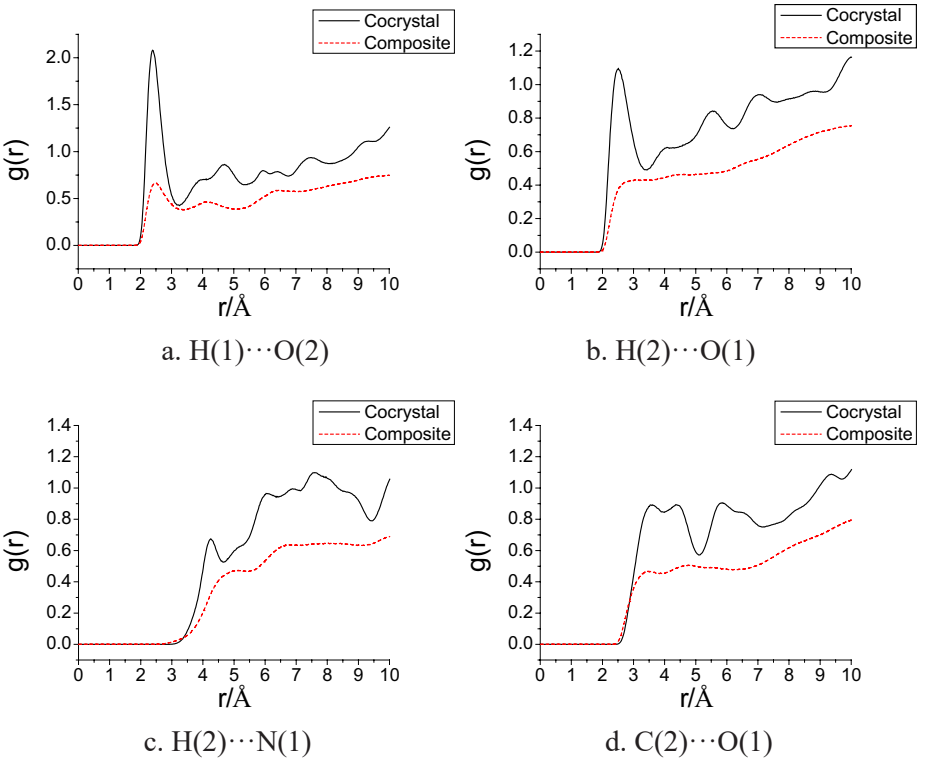

Figure 4. PCFs of H···O, H···N and C···O atom pairs in the CL-20/DNB co-crystal and composite at 295 K.

It is known that the usual interaction distance range (r) for a hydrogen bond is 2.0-3.1 Å, and for strong vdW is 3.1-5.0 Å. When r is longer than 5.0 Å, the vdW interaction is very weak [32]. In Figures 4a and 4b, the first peaks of the curves all locate at about 2.5 Å. This means that hydrogen bonds exist in the

H(1)···O(2) and H(2)···O(1) pairs. In Figure 4c, the first peak of the curves for H(2)···N(1) locate at about 4.2-4.9 Å, which indicates that the most significant part of the interaction in these atomic pairs is a vdW one. The nitro-aromatic interaction ordering in the co-crystal is shown in Figure 5, corresponding to the $g(r)$ curve in Figure 4d. The benzene ring of DNB has an electron deficient π-system due to the strong polarizing effect of the nitro groups, and one of the nitro groups of CL-20 lies almost above the center of the benzene ring of DNB. Therefore, a donor-acceptor p-π stacking interaction exists between the CL-20 nitro group and the electron-deficient benzene ring of DNB.

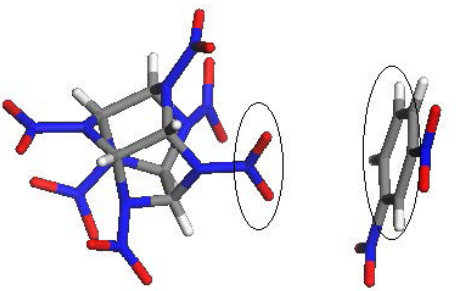

Figure 5. Nitro-aromatic interaction structure of CL-20 and DNB molecules in the co-crystal.

In Figures 4a-4d, we also found that the $g(r)$ value of the co-crystal is higher than that of the composite. This implies that the interaction between CL-20 and DNB in the co-crystal is stronger than that in the composite, which is consistent with the conclusion that E_{bind} of the CL-20/DNB co-crystal is much larger than that of the composite.

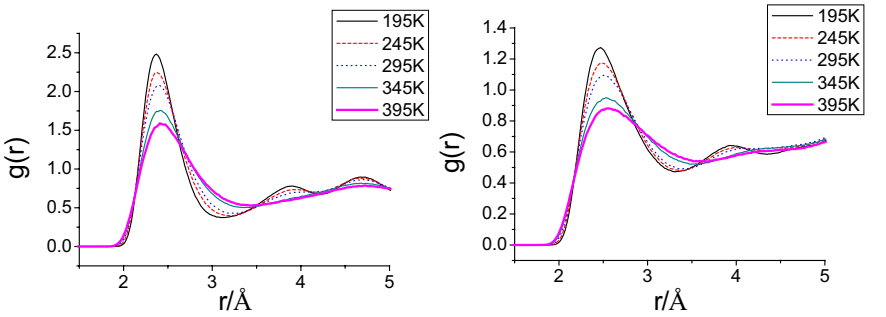

a. H(1)···O(2) b. H(2)···O(1)

Figure 6. PCF for (a) H(1)···O(2), and (b) H(2)···O(1) in the co-crystal at different temperatures.

Figure 6 shows the $g(r)$ values of H(1)···O(2) and H(2)···O(1) in the co-crystal, and their variation with temperature. The peak value obviously decreases and is slightly shifted to the right as the temperature increases. This is mainly attributed to the enhanced atomic motion at higher temperatures, and indicates that the interactions between CL-20 and DNB in the co-crystal decrease as the temperature increases. This conclusion agrees well with the trend that the binding energy of the co-crystal decreases at higher temperatures.

3.4 Mechanical properties of DNB crystals, ε-CL-20 crystals, the CL-20/DNB co-crystal and composite

Mechanical properties are some of the most important properties of energetic materials due to their relationship with material preparation, storage, transportation and usage. The elastic modulus is an indicator of material stiffness and a measurement of the material's resistance to elastic deformation. Plastic and fracture properties can be related to the elastic moduli. A higher shear modulus means greater hardness and more yield strength which reflect the resistance to plastic deformation. A higher bulk modulus means greater fracture strength. The quotient K/G indicates empirically the extent of the plastic range of a material. A high value of K/G is associated with ductility and a low value with brittleness [41]. The Cauchy pressure (C_{12}–C_{44}) [42] can also reflect the brittle/ductile behaviour. (C_{12}–C_{44}) is positive for a ductile material, and negative for a brittle material. The methodology of ductility evaluation using the Cauchy pressure based on the morphology of a fracture cross sectional surface is different from that of the K/G quotient [43].

Table 5 tabulates the predicted moduli, Poisson's ratios, quotients K/G and Cauchy pressures of the four models based on the fluctuation analysis of the production trajectories and the Reuss average [44, 45]. As the temperature increases, the elastic moduli of the four systems all decrease, indicating that their stiffness, hardness, yield strength and fracture strength are diminished at higher temperatures. For the same temperature, the moduli of the CL-20/DNB composite and co-crystal are smaller than those of the ε-CL-20 and DNB crystals, while the quotients K/G of the composite and the co-crystal are higher than those of the ε-CL-20 and DNB crystals. This indicates that the stiffness of both the composite and the co-crystal are lower, but their ductility is better. As the Cauchy pressure (C_{12}-C_{44}) values of DNB and ε-CL-20 crystals are negative, except for DNB at 195 K, and those of the CL-20/DNB composite and co-crystal are positive, the former are brittle materials and the latter are ductile ones. In addition, the Poisson's ratios of the co-crystal and the composite are larger than those of the two component crystals, indicating that the elastic elongations of the co-crystal and the composite are larger.

Table 5. Tensile modulus (E), Poisson's ratio (ν), bulk modulus (K), shear modulus (G), quotient K/G and Cauchy pressure (C_{12}-C_{44}) for DNB, CL-20/DNB composite and co-crystal, as well as ε-CL-20, at different temperatures. Deviations are listed in parenthesis. Units for E, K, G and C_{12}-C_{44} are GPa.

Model	Parameter	195 K	245 K	295 K	345 K	395 K
DNB	E	9.9 (0.0)	9.9 (0.0)	9.2 (0.0)	8.0 (0.0)	--
	ν	0.3 (0.0)	0.3 (0.0)	0.3 (0.0)	0.3 (0.0)	--
	K	8.0 (0.1)	7.5 (0.1)	6.7 (0.0)	6.0 (0.0)	--
	G	3.8 (0.0)	3.9 (0.0)	3.6 (0.0)	3.1 (0.0)	--
	K/G	2.1 (0.2)	1.9 (0.1)	1.8 (0.1)	1.9 (0.1)	--
	C_{12}-C_{44}	0.1 (0.0)	-0.4 (0.1)	-0.6 (0.1)	-0.7 (0.0)	--
Composite	E	5.3 (0.1)	4.8 (0.1)	4.0 (0.0)	3.5 (0.1)	--
	ν	0.4 (0.0)	0.4 (0.0)	0.4 (0.0)	0.4 (0.0)	--
	K	6.1 (0.1)	5.6 (0.1)	4.8 (0.0)	4.6 (0.1)	--
	G	2.0 (0.0)	1.8 (0.0)	1.5 (0.0)	1.3 (0.0)	--
	K/G	3.1 (0.1)	3.1 (0.1)	3.3 (0.1)	3.6 (0.2)	--
	C_{12}-C_{44}	3.4 (0.2)	3.2 (0.1)	2.7 (0.1)	2.5 (0.1)	--
Co-crystal	E	6.8 (0.1)	6.6 (0.1)	6.2 (0.0)	5.3 (0.1)	4.7 (0.0)
	ν	0.4 (0.0)	0.4 (0.0)	0.4 (0.0)	0.4 (0.0)	0.4 (0.0)
	K	7.9 (0.1)	7.8 (0.2)	7.1 (0.1)	7.0 (0.1)	6.5 (0.1)
	G	2.5 (0.0)	2.4 (0.0)	2.3 (0.0)	1.9 (0.0)	1.7 (0.0)
	K/G	3.2 (0.0)	3.2 (0.1)	3.1 (0.0)	3.6 (0.0)	3.8 (0.1)
	C_{12}-C_{44}	0.8 (0.1)	1.1 (0.2)	1.2 (0.1)	2.5 (0.1)	3.0 (0.1)
ε-CL-20	E	19.6 (0.0)	18.7 (0.1)	17.2 (0.1)	15.7 (0.1)	14.3 (0.1)
	ν	0.2 (0.0)	0.2 (0.0)	0.2 (0.0)	0.2 (0.0)	0.2 (0.0)
	K	11.5 (0.1)	11.3 (0.1)	10.5 (0.2)	9.7 (0.0)	8.9 (0.0)
	G	8.1 (0.0)	7.6 (0.0)	7.0 (0.0)	6.4 (0.0)	5.8 (0.0)
	K/G	1.4 (0.0)	1.5 (0.0)	1.5 (0.0)	1.5 (0.0)	1.5 (0.0)
	C_{12}-C_{44}	-6.4 (0.1)	-5.5 (0.2)	-5.3 (0.1)	-4.6 (0.2)	-4.1 (0.1)

Generally, a material of lower modulus implies that it deforms more easily and is able to disperse the energy applied to it, which makes it less sensitive. Due to the molecular arrangements and interactions in the composite and the co-crystal, they can easily exhibit elastic and plastic deformation, which is even larger than the deformation of the individual crystalline materials. On the other hand, for each material here, as the temperature increases, its sensitivity becomes higher although the modulus is reduced. This is because the temperature increase

imposes a straightforward and dominant influence on the movement of molecules, leading to more active molecules, easier reaction, and thus higher sensitivity.

4 Conclusions

In this study, NPT-MD simulations have been conducted for ε-CL-20, DNB, CL-20/DNB composite and co-crystal. The important findings may be summarized as follows.

(1) The L_{max} of the N−NO_2 trigger bond increases uniformly with increasing temperature. The L_{max} can be used as a theoretical criterion to judge the heat and impact sensitivity of the energetic system. L_{max} has also been compared between these materials at the same temperature. As a result, it is ranked as follows: CL-20/DNB(co-crystal) < CL-20/DNB(composite) < ε-CL-20 (crystal), indicating that the formation of the co-crystal can reduce the sensitivity and improve safety.

(2) The *CED*s of the CL-20/DNB co-crystal and composite both decrease with increasing temperature, suggesting that the energy needed for the transfer from the condensed phase to the gas phase can also be used to correlate with the heat and impact sensitivity. On the other hand, the *CED* of the co-crystal is higher than that of the composite under the same temperature conditions, indicating that the co-crystal system is more stable and insensitive than the ordinary composite, which implies that co-crystallization of CL-20 with DNB can reduce sensitivity.

(3) The E_{bind} between CL-20 and DNB decreases with increasing temperature. The E_{bind} of the CL-20/DNB co-crystal is much larger than that of the composite, because the interaction between the different components in the co-crystal exists between the layers having larger interaction areas, while for the composite, the interaction areas are smaller. The pair correlation function $g(r)$ reveals that the hydrogen bonded interactions in the co-crystal and the composite mainly comes from the H of CL-20 and the O of DNB, the H of DNB and the O of CL-20, and decrease slightly as the temperature increases. Additionally, a donor-acceptor p-π stacking interaction exists between the CL-20 nitro group and the electron-deficient benzene ring of DNB.

(4) Compared with those of the ε-CL-20 and DNB crystals, we found that the moduli of the CL-20/DNB co-crystal and composite are smaller, while their K/G quotients are larger, and the Cauchy pressure (C_{12}-C_{44}) values are positive, indicating that the stiffness of the co-crystal and the composite are smaller, but their ductility is better. In addition, the elastic elongations of the CL-20/DNB co-crystal and composite are larger because of the higher Poisson's ratios.

Acknowledgement
This work is supported by a grant from the Joint Fund of National Natural Science Foundation of China and the China Academy of Engineering Physics (NSAF) (Grant No. U1230120) and a grant from the National Natural Science Foundation of China (Grant No. 11572160).

References

[1] Agrawal J.P., Recent Trends in High-Energy Materials, *Prog. Energy Combust. Sci.*, **1998**, *24*(1), 1-30.
[2] Sikder A.K, Sikder N., A Review of Advanced High Performance, Insensitive and Thermally Stable Energetic Materials Emerging for Military and Space Applications, *J. Hazard. Mater*., **2004**, *112*(1), 1-15.
[3] Landenberger K.B., Matzger A.J., Cocrystal Engineering of a Prototype Energetic Material: Supramolecular Chemistry of 2,4,6-Trinitrotoluene, *Cryst. Growth & Design*, **2010**, *10*(12), 5341-5347.
[4] Shen J P, Duan X H, Luo Q P, Zhou Y, Bao Q L, Ma Y J, Pei C H. Preparation and Characterization of a Novel Cocrystal Explosive, *Cryst. Growth Des.*, **2011**, *11*(5): 1759-1765.
[5] Bolton O, Matzger A J. Improved Stability and Smart-material Functionality Realized in an Energetic Cocrystal, *Angew. Chem., Int. Ed.*, **2011**, *50*(38), 8960-8963.
[6] Bolton O., Simke L.R., Pagoria P.F., Matzger A.J., High Power Explosive with Good Sensitivity: A 2:1 Cocrystal of CL-20:HMX, *Cryst. Growth Des.*, **2012**, *12*(9), 4311-4314.
[7] Landenberger K.B., Matzger A.J., Cocrystals of 1,3,5,7-Tetranitro-1,3,5,7-tetrazacyclooctane (HMX), *Cryst. Growth Des.*, **2012**, *12*(7), 3603-3609.
[8] Guo C.Y, Zhang H B, Wang X.C., Liu X.F., Sun J., Study on a Novel Energetic Cocrystal of TNT/TNB, *J. Mater. Sci*., **2013**, *48*(3): 1351-1357.
[9] Zhang H.B., Guo C.Y., Wang X.C., Xu J.J., He X., Liu Y., Liu X.F., Huang H., Sun J., Five Energetic Cocrystals of BTF by Intermolecular Hydrogen Bond and π-Stacking Interactions, *Cryst.Growth Des.*, **2013**, *13*(2), 679-687.
[10] Millar D.I.A., Maynard-Casely H.E., Allan D.R., Cumming A.S., Lennie A.R., Mackay A.J., Oswald I.D.H., Tang C.C., Pulham C.R., Crystal Engineering of Energetic Materials: Co-crystals of CL-20, *Cryst. Eng. Comm*., **2012**, *14*(10), 3742-3749.
[11] Yang Z.W., Li H.Z., Zhou X.Q., Zhang C.Y., Huang H., Li J.S., Nie F.D., Characterization and Properties of a Novel Energetic-Energetic Cocrystal Explosive Composed of HNIW and BTF, *Cryst. Growth Des.*, **2012**, *12*(11), 5155-5158.
[12] Yang Z.W., Li H.Z., Huang H., Zhou X.Q, Li J.S., Nie F.D., Preparation and Performance of a HNIW/TNT Cocrystal Explosive, *Propellants Explos. Pyrotech.*,

2013, *38*(4), 495-501.
[13] Guo C.Y., Zhang H.B., Wang X.C., Xu J.J., Liu Y., Liu X.F., Huang H., Sun J., Crystal Structure and Explosive Performance of a New CL-20/Caprolactam Cocrystal, *J. Mol. Struct*., **2013**, *1048*, 267-273.
[14] Wang Y.P., Yang Z.W., Li H.Z., Zhou X.Q., Zhang Q., Wang J.H., Liu Y.C., A Novel Cocrystal Explosive of HNIW with Good Comprehensive Properties, *Propellants Explos. Pyrotech*., **2014**, *39*(4), 590-596.
[15] Maksimowski P., Rumianowski T., Properties of the Gamma-Cyclodextrin/CL-20 System, *Centr. Eur. J. Energ. Mater*., **2016**, *13*(1), 217-229.
[16] Lara-Ochoa F., Espinosa-Perez G., Cocrystals Definitions, *Supramolecular Chemistry*, **2007**, *19*(8), 553-557.
[17] Shan N., Zaworotko M.J., The Role of Cocrystals in Pharmaceutical Science, *Drug Discovery Today*, **2008**, *13*(9), 440-446.
[18] Agrawal J.P., Some New High Energy Materials and Their Formulations for Specialized Applications, *Propellants Explos. Pyrotech.*, **2005**, *30*(5), 316-328.
[19] Foltz M.F., Coon C.L., Garcia F., Nichols A.L. The Thermal Stability of the Polymorphs of Hexanitrohexaazaisowurtzitane, Part I., *Propellants Explos. Pyrotech.*, **1994**, *19*(1), 19-25.
[20] Xiao H.M., Xu X.J., Qiu L., *Theoretical Design of High Energy Density Materials*, Beijing, Science Press, **2008**.
[21] Zhong Y.P., Hu Y.D., Jiang H.Z., *Handbook for Properties of Explosives* (in Chinese), Ordnance Industry Press, Beijing, **1990**.
[22] Sun H., COMPASS: An Ab Initio Force-field Optimized for Condensed-phase Applications Overview with Details on Alkane and Benzene Compounds, *J. Phys. Chem. B*, **1998**, *102*(38), 7338-7364.
[23] Bunte S.W., Sun H., Molecular Modeling of Energetic Materials: the Parameterization and Validation of Nitrate Esters in the COMPASS Force Field, *J. Phys. Chem. B*, **2000**, *104*(11), 2477-2489.
[24] Zhao X.Q., Shi N.C., Crystal Structure of ε-Hexanitrohexaazaisowurtzitane, *Chin. Sci. Bull.*, **1995**, *40*(23), 2158-2160.
[25] Trotter J, Williston C S. Bond Lengths and Thermal Vibrations in m-Dinitrobenzene, *Acta Crystallogr.*, **1966**, *21*(2), 285-288.
[26] Andersen H.C., Molecular Dynamics Simulations at Constant Pressure and/or Temperature, *J. Chem. Phys*., **1980**, *72*(4), 2384.
[27] Parrinello M., Rahman A., Polymorphic Transitions in Single Crystals: A New Molecular Dynamics Method, *J. Appl. Phys.*, **1981**, *52*, 7182.
[28] Allen M.P., Tildesley D.J., *Computer Simulation of Liquids*, Oxford University Press, **1989**.
[29] Ewald P.P., Evaluation of Optical and Electrostatic Lattice Potentials, *Ann. Phys.*, **1921**, *64*, 253-287.
[30] Politzer P., Murray J.S., Lane P., Sjoberg P., Adolph H.G., Shock-sensitivity Relationships for Nitramines and Nitroaliphatics, *Chem. Phys. Lett.*, **1991**, *181*(1), 78-82.

[31] Patil D.G., Brill T.B., Thermal Decomposition of Energetic Materials 53. Kinetics and Mechanism of Thermolysis of Hexanitrohexazaisowurtzitane, *Combust. Flame*, **1991**, *87*(2), 145-151.
[32] Korsounskii B.L., Nedel'ko V.V., Chukanov N.V., Larikova T.S., Volk F., Kinetics of Thermal Decomposition of Hexanitrohexaazaisowurtzitane, *Russ. Chem. Bull.*, **2000**, *49*(5), 812-818.
[33] Geetha M., Nair U.R., Sarwade D.B., Gore G M, Asthana S.N., Singh H., Studies on CL-20: the Most Powerful High Energy Material, *J. Therm. Anal. Calorim.*, **2003**, *73*(3), 913-922.
[34] Xu X.J., Xiao H.M., Ju X.H., Gong X.D., Theoretical Study on Pyrolysis Mechanism for ε-Hexanitrohexaazaisowurtzitane, *Chinese Journal of Organic Chemistry (Youji Huaxue)*, **2005**, *25*(5), 536-539.
[35] Xu X.J., Zhu W.H., Xiao H.M., DFT Studies on the Four Polymorphs of Crystalline CL-20 and the Influences of Hydrostatic Pressure on ε-CL-20 Crystal, *J. Phys. Chem. B*, **2007**, *111*(8), 2090-2097.
[36] Xiao J.J., Zhao L., Zhu W., Chen J., Ji G.F., Zhao F., Wu Q., Xiao H.M., Molecular Dynamics Study on the Relationships of Modeling, Structural and Energy Properties with Sensitivity for RDX-based PBXs, *Sci. China: Chem.*, **2012**, *55*(12), 2587-2594.
[37] Xiao J.J., Wang W.R., Chen J., Ji G.F., Zhu W., Xiao H.M., Study on Structure, Sensitivity and Mechanical Properties of HMX and HMX-based PBXs with Molecular Dynamics Simulation, *Comput. Theor. Chem.*, **2012**, *999*, 21-27.
[38] Xiao J.J., Zhu W.H., Zhu W., Xiao H.M., *Molecular Dynamics of Energetic Materials*, Beijing: Science Press, **2013**.
[39] Politzer P., Murray J.S., Quantitative Analyses of Molecular Surface Electrostatic Potentials in Relation to Hydrogen Bonding and Co-crystallization, *Crys. Growth Des.*, **2015**, *15*, 3767-3774.
[40] Murray J.S., Shields Z.P., Seybold P.G., Politzer P., Intuitive and Counterintuitive Noncovalent Interactions of Aromatic π Regions with the Hydrogen and the Nitrogen of HCN, *J. Comput. Sci.*, **2015**, *10*, 209-216.
[41] Pugh S.F., Relations between the Elastic Moduli and the Plastic Properties of Polycrystalline Pure Metals, *Philos. Mag.*, **1954**, *45*(367), 823-843.
[42] Pettifor D.G., Theoretical Predictions of Structure and Related Properties of Intermetallics, *Mater. Sci. Technol.*, **1992**, *8*(4), 345-349.
[43] Xiao J.J., Wang W.R., Chen J., Ji G.F., Zhu W., Xiao H.M., Study on Structure, Sensitivity and Mechanical Properties of HMX and HMX-based PBXs with Molecular Dynamics Simulation, *Comput. Theor. Chem.*, **2012**, *999*, 21-27.
[44] Parrinello M., Rahman A., Strain Fluctuations and Elastic Constants, *J. Chem. Phys*., **1982**, *76*(5), 2662-2666.
[45] Watt J.P., Davies G.F., O'Connell R.J., The Elastic Properties of Composite Materials, *Rev. Geophys.*, **1976**, *14*(4), 541-563.